防蝕工程　第二十卷第一期　第89～110頁　2006年3月
Journal of Chinese Corrosion Engineering, Vol.20 No.1, PP. 89~110 (2006)

敏化之304型不銹鋼在模擬沸水式反應器環境中的疲勞裂縫成長行為

陳彥羽*[1]、施漢章[1]、王立華[2]、翁榮洲[2]、賴玄金[2]

Fatigue Crack Growth Behavior of Sensitized Type 304 Stainless Steel in Simulated Boiling Water Reactor Environments

Y. Y. Chen*[1], H. C. Shih[1], L. H. Wang[2], J. C. Oung[2], H. C. Lai[2]

摘 要

本論文使用破壞力學標準緊緻拉伸試片，研究電化學電位再活化值為30 C/cm²的敏化304型不銹鋼，在288 ºC之模擬沸水式反應器環境中的疲勞裂縫生長速率行為。試驗以週期式或梯形負荷條件來進行。試驗環境為含有200 ppb溶氧的正常水化學或含有10 ppb溶氧與160 ppb溶氫的加氫水化學之純水。結果發現：敏化之304不銹鋼在高溫水中的電化學腐蝕電位與溶氧及溶氫量有密切的關係。然而，不論負荷形式為週期式或梯形，加氫水化學均無法減緩裂縫成長速率。實驗量測到的裂縫成長速率均無法被ASME法規第十一節之附錄C的參考曲線所涵蓋，而所有數據卻均可被JSME之裂縫估算法規所規範。最後，結果亦顯示阿岡諾國家實驗室對於不銹鋼在高溫純水中的裂縫成長速率之預測模型的準確性高於奇異公司所發展之預測模型。

關鍵詞：腐蝕疲勞；304型不銹鋼；沸水式反應器；裂縫成長速率；加氫水化學。

ABSTRACT

The fatigue crack growth rate (FCGR) behaviors of sensitized Type 304 stainless steel (304 SS) with an electrochemical potentiokinetic reactivation (EPR) value of 30 C/cm^2 was investigated using fracture mechanics-type standard compact tension (CT) specimens in simulated boiling water reactor (BWR) environments at 288ºC. Tests were performed under either cyclic or trapezoidal loading conditions. Test environments were pure water either with 200 ppb dissolved oxygen (DO) under normal water chemistry (NWC) conditions or with 10 ppb DO plus 160 ppb dissolved hydrogen (DH) under hydrogen water chemistry (HWC) conditions. The electrochemical corrosion potential (ECP) of sensitized 304 SS in high-temperature pure water was found to be closely related to the amounts

1 國立清華大學材料科學與工程學系
Department of Materials Science and Engineering, National Tsing Hua University.
2 工業技術研究院工業材料研究所
Materials Research Laboratories, Industrial Technology Research Institute.
* 連絡作者：franklin_chen_1@hotmail.com

of DO and DH. However, it was observed that whether the loading waveform was cyclic or trapezoidal, the CGRs could not be reduced by HWC conditions. None of the current CGR data was encompassed by the reference curves of the ASME Code Section XI, Appendix C (ASME-XI, Appendix C), whereas all of the current data could be bounded by the JSME flaw evaluation code (JSME S NA1-2000). Finally, the examination of the accuracy of the superposition principles indicated that the Argonne National Laboratory (ANL)-model was higher than that developed by the General Electric (GE)-model.

Keywords: Corrosion fatigue; Type 304 stainless steel; Boiling water reactor; Crack growth rate; Hydrogen water chemistry.

1. Introduction

Since the 1970s, a number of studies have shown that for the structural materials used in nuclear power plant, such as carbon steels (CSs), low-alloy steels (LASs), and austenitic stainless steels (SSs), the fatigue lifetime will be reduced and the crack growth rate (CGR) will be accelerated if these materials are exposed to high-temperature water[1~2]. In general, this phenomenon is called environmentally assisted cracking (EAC), and the mechanisms of EAC can be divided into the three categories: corrosion fatigue (CF), stress corrosion cracking (SCC), and strain-induced corrosion cracking (SICC).

Austenitic SSs are used extensively as structural alloys in reactor–pressure–vessel (RPV) internal components because of their high strength, ductility, and fracture toughness. Over the previous three decades, EAC of austenitic SSs (e.g., Type 304 SS and Type 316 SS) in high-temperature water has been the key subject of worldwide investigations, primarily as a result of events of intergranular cracking (IGC) in light water reactors (LWRs)[3~14]. Cracking was initially due to chromium (Cr) depletion at grain boundaries (GBs), which takes place as chromium carbides (mainly $Cr_{23}C_6$) nucleate and grow in the GBs. When the carbides grow, the carbon rapidly diffuses to the interface between carbide and matrix and is available to the growing carbide. Since Cr diffuses much more slowly, it is obtained from the surrounding material, which then becomes depleted of Cr (sensitized), and thus is more susceptible to corrosive attack. Because the carbides preferentially form along the GBs, corrosion and EAC are often intergranular.

Recently, reactor water chemistry improvements, such as reducing the dissolved oxygen (DO) concentration, have been considered good countermeasures to EAC in structural materials in boiling water reactor (BWR) plants. Hydrogen (H_2) addition to reactor feedwater, creating hydrogen water chemistry (HWC), has been applied largely in primary SS piping systems of commercial BWR plants[15~17]. However, some laboratories such as the Argonne National Laboratory (ANL)[18~19] and the Ishikawagima-Harima Heavy Industries (IHI)[20] observed that the fatigue lives of SSs (e.g., 304 SS and 316 nuclear grade [NG] SS) in high-temperature (288 °C) water with low DO (or low electrochemical corrosion potential [ECP]) environments were even much shorter than those under high DO (or high ECP) conditions. In addition, Van der Sluys and Yukawa[21~22] also found that environmental effects on the fatigue lifetimes of austenitic SSs are more pronounced in low-DO than in high-DO water. Such a dependence of fatigue life on DO content is quite different from that of ferritic steels. For CSs and LASs, environmental effects on fatigue lifetimes increase with the increase of DO content

above a minimum threshold value of 0.05 ppm in high-temperature water[23~24]. Therefore, more test data are necessary in order to further confirm whether CGRs of SSs will be suppressed under HWC conditions (low DO or low ECP) or not.

In addition, many models which combine fatigue and stress corrosion effects have been suggested for use in predicting the CGR as a function of fatigue loading frequency. These models can be divided into three types as follows: (1) superposition model[25], (2) competition model[26], and (3) models involving environmentally modified materials deformation and fatigue properties[27~30]. The superposition model and the competition model both make the assumption that an environmental fracture process is independent of the mechanical fatigue fracture process and that the mechanical fatigue fracture process in a corrosive environment is identical with the process in an inert environment[25~26]. Environmental degradation and a pure fatigue fracture process occur simultaneously and independently on the same fracture surface, and have no interaction with each other according to the superposition model[25]. Therefore, the total CF CGR ($(da/dN)_{CF}$) is the linear addition of each contribution attributed to the environmental fracture process ($(da/dN)_{SCC}$) and the mechanical fracture process ($(da/dN)_{inert}$). The superposition model has explained the CF crack growth behavior relatively well for some CF systems and also has been used for predicting the lifetime of structural materials in nuclear reactors. However, there are still numerous cases in which the superposition model cannot be applied suitably[31~35].

In this study, we obtain useful CGR data of sensitized 304 SS under either normal water chemistry (NWC) or HWC in simulated BWR environments in order to compare these data with some well-known predictive models like the ASME Code Section XI, Appendix C (ASME-XI, Appendix C)[36], the JSME (Japan Society of Mechanical Engineers) flaw evaluation code (JSME S NA1-2000)[37], the PLEDGE (Plant Life Extension Diagnosis by General Electric) model (GE-model)[38~39], and the ANL-model[40~41]. In addition, we have attempted to gain further understanding of whether or not the presence of dissolved hydrogen (DH) under BWR conditions will suppress the CGR of sensitized 304 SS. Finally, besides a positive saw tooth cyclic loading, a trapezoidal loading composed of cyclic and constant loading periods was also used to examine the accuracy of superposition principles developed by the GE-model and the ANL-model.

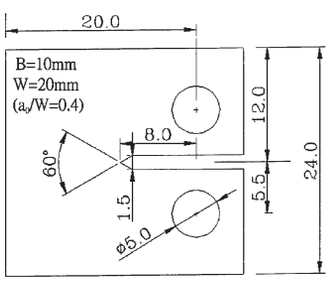

圖1　厚度為10 mm且無側表面溝槽之標準緊緻拉伸試片。

Figure 1　Standard compact tension (CT) specimens with thickness of 10 mm (~0.4T-C(T)) without side grooves.

表1.　本研究所使用之304型不銹鋼的化學成分 (wt%)。

Table 1　Chemical compositions of Type 304 SS used in this study (wt.%).

C	Si	Mn	P	S	Ni	Cr	Fe
0.06	0.29	0.79	0.032	0.023	8.14	18.18	Balance

2. Experimental procedures

2.1 Test materials and specimens

10-mm-thick fracture mechanics-type standard compact tension specimens (~0.4 T-CT) without side grooves, as shown in Figure 1, were machined from a hot-rolled Type 304 stainless steel (304 SS) plate with the crack extension direction perpendicular to the rolling direction of the plate. The actual chemical composition of the 304 SS used in this study was determined by glow discharge-optical emission spectrograph (GD-OES), as listed in Table1. Prior to CF testing, all specimens were solution annealed (SA) at 1100 °C for one hour and water quenched (WQ). Subsequently, the specimens were furnace sensitized (FS) at 620 °C for 24 h and air cooled (AC). Sensitization levels were measured using the electrochemical potentiokinetic reactivation (EPR) technique described in the Japan Industrial Standard (JIS) G 0580[42]. The EPR value (ratio of anodic current densities in double-loop scans) for the sensitized specimens was 30 C/cm^2.

Each CT specimen was fatigue precracked beyond the original machined notch under a sinusoidal waveform with a frequency of 15 Hz and a stress ratio (R) of 0.5 using a 5 ton capacity servo-hydraulic (INSTRON 8500) dynamic material tester in air at room temperature (~ 25 °C). The maximum stress intensity factor, K_I, at the final load step was lower than 20 MPa√m. The specimen scale and precrack procedures all complied with the rules specified by ASME E 399[43]. After precracking, the specimen surfaces were polished with a 1500-grit emery paper and cleaned in an ultrasonic bath with distilled water for ~ 5 minutes, and then dried in air.

2.2 Water chemistry and environmental parameters

The CF tests were conducted in circulated high temperature water loops, as shown in Figure 2. Water chemistries were measured at the inlet and outlet of the autoclave using a water resistivity meter (Thornton Type 822), a low dissolved O_2 (DO) monitor (Orion 1808), and a dissolved H_2 (DH)

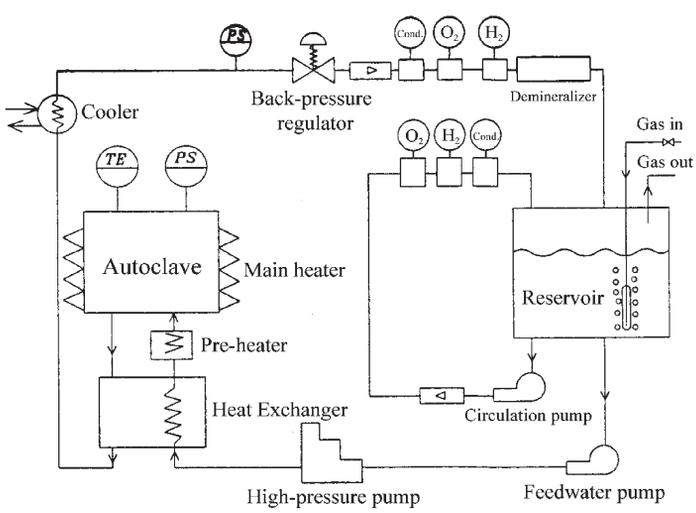

圖2　循環高溫水迴路之示意圖。

Figure 2　Schematic representation of circulation of the high temperature water loops.

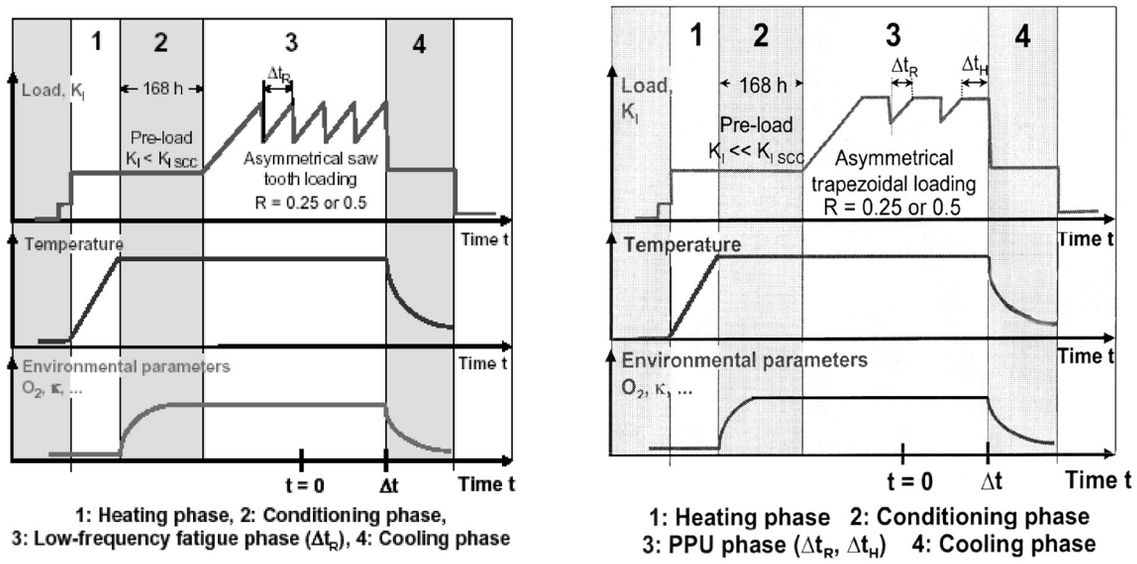

圖3　實驗進行示意圖：(a) 疲勞裂縫生長試驗(非對稱鋸齒負荷)，與 (b) 疲勞裂縫生長試驗(非對稱梯形負荷)[45~46] 。

Figure 3　Schematic representation of test procedure diagram: (a) FCGR tests (asymmetrical saw tooth loading), and (b) FCGR tests (asymmetrical trapezoidal loading)[45~46].

monitor (Orbisphere Model 3600). Conductivity and concentrations of DO or DH were controlled at the autoclave inlet. The influent water conductivity was always ~0.06 μS/cm, and the effluent was typically < 0.08 μS/cm, at ambient temperature.

A 2-liter, Type 316 (UNS S31600) stainless steel autoclave, fitted with a recuperative heat exchanger was fed by a feedwater pump in series with a high-pressure pump, which provided a flow rate of 6 L/h. That is, the water in the autoclave was exchanged three times per hour. A mixture of re-circulating and make-up water was purified and demineralized by passage through a nuclear grade (NG) ion exchanger. DO and DH were controlled by sparging the water in the reservoir with nitrogen containing the appropriate partial pressures of oxygen or hydrogen. The gas flow rates were controlled by a flow-controller, to establish the desired water chemistry. To avoid galvanic effects, the specimens were electrically insulated from the autoclave by polytetrafluoroethylene (PTFE) and from the clip gauges by thermally sprayed zirconium oxide (ZrO_2) spacers.

The ECP of each specimen was continuously monitored by use of a zirconia/copper/cuprous oxide (ZrO_2/Cu/Cu_2O) high-temperature reference electrode and converted to the standard hydrogen electrode (SHE) on the basis of the calculated potential for the ZrO_2 sensor in neutral water[44]. The pH value in the system was between 5.6 and 5.8 at 288 °C (~ 561K) as measured by a GLI Model 53 pH-meter.

2.3 Test conditions and mechanical loading

After installing a pre-cracked specimen, the autoclave was filled with pure water, bubbled with

nitrogen to remove excessive oxygen, and then heated up to 288 °C. To achieve stable conditions with respect to water chemistry, electrochemistry, and oxide film formation, the specimens were pre-oxidized and subjected to a pre-load of approximately 9 kN for at least 168 h (1 week) prior to initiating the CF test. The normal test environment was pressurized (about 8.0 MPa), high-temperature, high-purity water at 288 °C with a nominal inlet DO content of 200 ppb, i.e., NWC conditions. In addition, some specimens were tested under both NWC and HWC (10 ppb DO + 160 ppb DH) conditions.

The CF tests were conducted under tension-to-tension load controlled modes with an R value of either 0.25 or 0.5. The load waveform in some tests was an asymmetrical positive saw tooth (slow loading, fast unloading)[45], as shown in Figure 3(a), with a frequency of either 410^{-3} Hz (rise time 230 s, fall time 20 s) or 4×10^{-4} Hz (rise time 2300 s, fall time 200 s). Specimens were loaded to nominal initial ΔK values of 10-20 MPa√m, calculated according to the equation in ASTM E 399[43]. On the other hand, some CF tests were carried out using asymmetrical trapezoidal waves under dynamic load control modes[46~47], as shown in Figure 3(b). Trapezoidal waves were composed by holding for different periods (Δt_H) at the top (maximum) load.

After several hundred to two thousand hours of testing, the specimens were unloaded to 9 kN, the heating was stopped, and the pressure was gradually decreased. The specimens were disassembled, cleaned in an ultrasonic bath with distilled water and dried. The specimens were then broken apart by fatigue at room temperature in air to allow post-test observation of the fracture surfaces. Both the test conditions and simulated BWR water chemistries are summarized in Table 2.

2.4 On-line crack growth monitoring and fractographical post-test observation

Crack propagation in each individual specimen was monitored continuously on-line using the

表2.　測試條件與模擬沸水式反應器之水化學規格。
Table 2　Test conditions and simulated BWR water chemistry specifications.

Test conditions and water chemistry for fatigue crack growth		
Materials	Sensitized Type 304 SS	
Specimens	Compact Tension (B = 10mm, W = 20mm)	
Control mode	Load Control	
Stress ratio (R)	0.25 or 0.5	
Frequency	4×10^{-3} Hz, 4×10^{-4} Hz	
Waveform	Asymmetrical positive saw tooth or Asymmetrical trapezoidal	
Temperature	288 ± 0.5 °C (~ 561 K)	
Pressure	1100 psi (~ 8.0 MPa)	
Water chemistry	**NWC**	**HWC**
DO	200 ± 10 ppb	10 ± 0.5 ppb
DH	0	160 ± 5 ppb
pH	5.7 ± 0.1	
Conductivity	< 0.06 μS/cm (inlet) < 0.08 μS/cm (outlet)	

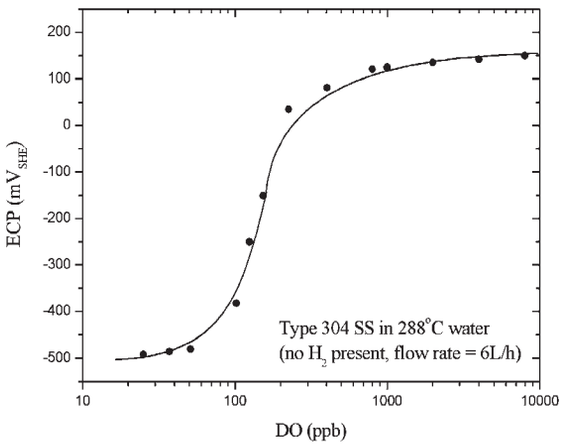

圖4　304型不銹鋼在288 °C高純度且流速為每小時6公升之水中，溶氧對的電化學腐蝕電位的影響。電化學腐蝕電位是隨著溶氧增加的方向依序量測所得。

Figure 4　Effect of DO on the ECPs of Type 304 SS in 288 °C high-purity water at a flow rate of 6 L/h. The ECP was measured as DO was increased.

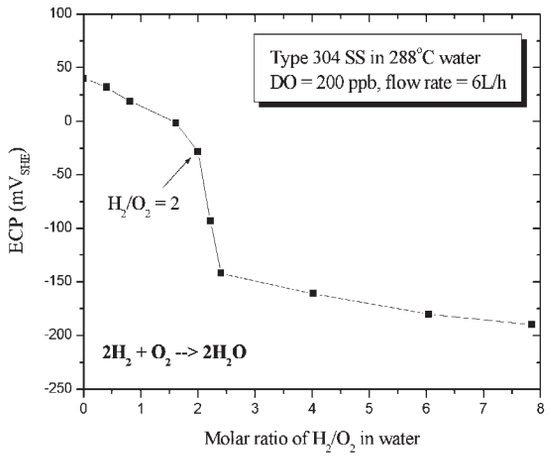

圖5　304型不銹鋼在288 °C，含氧量200 ppb之高純度水中，電化學腐蝕電位隨著氫氣與氧氣之莫爾比而變化的情形。水流速率為每小時6公升。

Figure 5　ECP behavior of Type 304 SS in 288°C high-purity water containing 200 ppb O_2 as a function of the molar ratio of H_2 to O_2. Flow rate was 6 L/h.

reverse direct-current potential drop (RDC-PD) method according to ASTM E 647[48]. The potential drop across the crack mouth was measured while a constant current of 3 amperes flowed through the specimen. The polarity of the current was reversed about once per second in order to reduce errors associated with thermoelectric and amplifier offsets. Many potential drop readings were averaged and then related to crack length through polynomial fits. The results were verified by comparison with extensive post-test fractography evaluations by scanning electron microscopy (SEM). The evaluated RDC-PD resolution limit corresponded to roughly 5 to 10 μm (depending to test conditions)[49].

After testing, fractographic examination of all test specimens was performed. Crack extension distances were measured on both sides of a specimen. For the fatigue-tested specimens, although the difference between calculated and fractographically determined increment of crack advance was found to be < 5%, data from the fractographic examination were taken as the final result when there was a discrepancy between this crack length determination and the RDC-PD data. These measurements of crack lengths allowed calculation of the cycle-dependent CGR, $\Delta a/\Delta N$, and the time-dependent CGR, $(\Delta a/\Delta N)/\Delta t_R$ (Δt_R = rise time, see Figure 3(a)). The correlation coefficients from linear regression analyses of the crack length vs. time data from which growth rates were calculated were typically > 0.95. These data were then compared with CGR values estimated from some predictive models.

3. Results and discussion

3.1 Effects of DO and DH on ECP

The effects of DO and DH on the ECPs of sensitized 304 SS are shown in Figures 4 and 5,

respectively. Specimens were immersed (pre-filmed) in 288 °C high-purity water containing 200 ppb O_2 for 7 days. The ECP was first measured after an incremental addition of O_2. Then, the specimen was left for 3 days in 288 °C water without any further addition of O_2 or H_2 to let the ECP stabilize. Subsequently, an incremental addition of H_2 was made to this water, which already contained 200 ppb O_2. It is worth noting that a much longer period was required for the ECP to stabilize after this addition of H_2 than after the previous addition of O_2. This may indicate that the H_2 addition caused a slow transformation of the oxide layer from Fe_2O_3 phase to Fe_3O_4[50~51].

A plot of the steady-state ECPs for sensitized 304 SS, as a function of oxygen concentration at a flow rate of 6 L/h (100 cc./min), is shown in Figure 4. In Figure 4, a significant increase in the ECP can be observed in the oxygen concentration range between 50 and 400 ppb. Above 800 ppb, the ECP is approximately proportional to the logarithm of the DO with a slope of ~30 mV/decade DO. In addition, the inflection point occurs at an oxygen concentration of 150 ppb, whereas those obtained by Macdonald et al.[52] and Indig and McIlree[53] occur at 200 ppb and 20-40 ppb, respectively. The differences of the ECPs may be attributed to the type of reference electrode used, the distance between the reference electrode and the specimen, the flow rate, the degree of sensitization, and/or the instrumentation.

It is worth noting that the ECP vs. DO curve for the sensitized 304 SS used in this study shows the typical S-shaped (sigmoid) form, similar to the results obtained by some earlier studies[52~54]. According to these studies, the S-shaped curves were generally measured in an autoclave with very slow water flow (e.g., 20 cc./min in Reference 52, 100 cc./min in Reference 53, and 10 cm^3/min in Reference 54). On the other hand, at a higher flow rate (2.2 kg/min), a gradual increase in the ECPs, instead of the S-shaped curve, was observed between

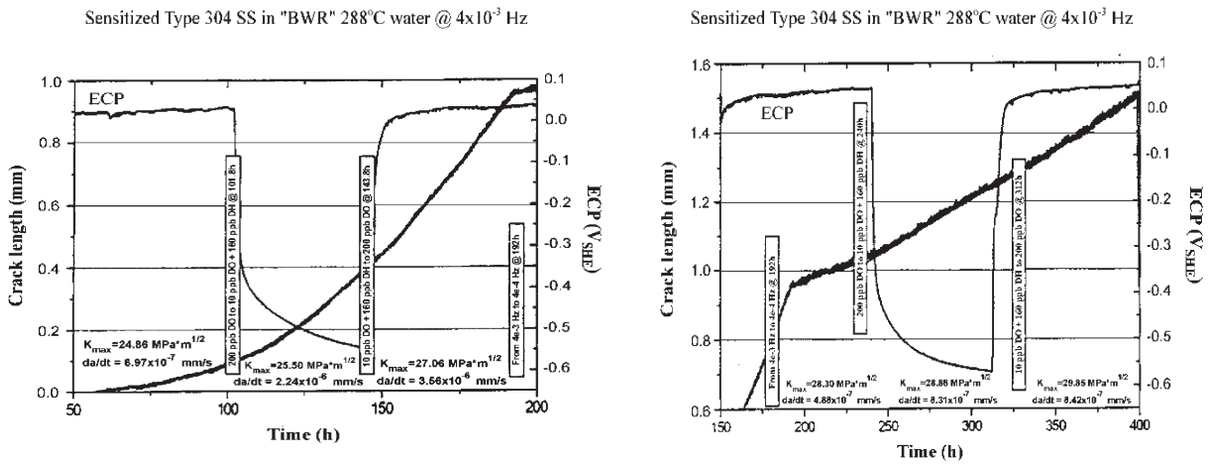

(a)　　(b)

圖6　敏化之304型不銹鋼試片測試於負荷頻率為(a) 4×10^{-3}赫茲(正常水化學→加氫水化學→正常水化學)，與 (b) 4×10^{-4}赫茲(正常水化學→加氫水化學→正常水化學)的條件下，裂縫成長速率在288 °C水中隨時間的變化情形。

Figure 6　CGR as a function of time for a sensitized Type 304 SS specimen tested at 288°C water under cyclic loading (a) at 4×10^{-3} Hz (NWC→HWC→NWC), and (b) at 4×10^{-4} Hz (NWC→HWC→NWC).

0.1 and 1000 ppb of O_2[55]. The sigmoid relationship between ECP and DO shown in Figure 4 may occur because of a transition between two different cathodic reactions. In high-temperature low-DO water, the controlling cathodic process is possibly the direct reduction of water by the following reaction:

$$2e^- + 2H_2O \rightarrow 2OH^- + H_2 \quad (1)$$

On the other hand, the cathodic process in high-DO water is probably the reduction of oxygen according to the following reaction:

$$4e^- + O_2 + 4H^+ \rightarrow 2H_2O \quad (2)$$

In the intermediate range of DO, the shift in cathodic reactions could significantly influence both the ECP and the tendency for IGSCC[53].

Figure 5 shows the ECP behavior of 304 SS in 288 °C high-purity water containing 200 ppb O_2 as a function of the molar ratio of H_2 to O_2. Similar to the results in our previous study[56], it was observed that ECP can effectively be lowered by adding a trace amount of H_2 (e.g., 10 ppb). For instance, the ECP drops significantly from ~ 0 mV_{SHE} to ~ -200 mV_{SHE} as the molar ratio of H_2 to O_2 increases from 1.62 to 7.85. There is a sudden drop in the ECP value as the H_2/O_2 molar ratio increased from 2.00 to 2.41 but, when the H_2/O_2 molar ratio > 2.41, the decrease of the ECP tends to be more gradual. A H_2/O_2 molar ratio of 2 implies that all of the DH (25 ppb) may completely react with the DO (200 ppb) to form water by the reaction as follows:

$$2H_2 + O_2 \rightarrow 2H_2O \quad (3)$$

That is, 2 moles of hydrogen can react with 1 mole of oxygen to form 2 moles of water in high temperature neutral water. Then, as the H_2/O_2 molar ratio drops below 2, the hydrogen is all used up to decrease the ECP value.

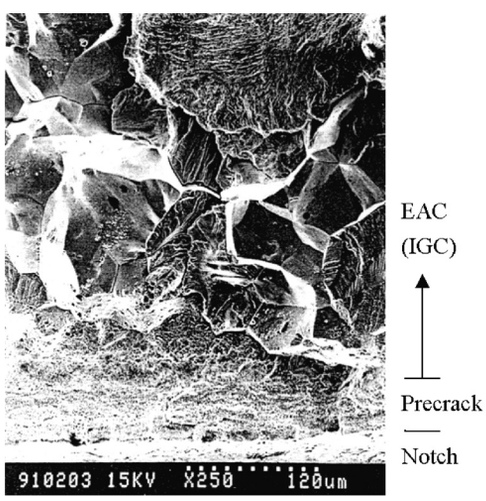

圖7　破裂面的掃瞄式電子顯微鏡照片顯示破裂面之破裂模式為混合型，亦即裂縫在預裂階段主要是屬穿晶破裂的形式，而在高溫水中的裂縫成長階段則主要是沿晶破裂的形式。而此圖中裂縫延伸的方向為由下往上。

Figure 7　SEM photograph showing mixed mode fracture morphology with transgranular cracking dominating in the precracking stage and intergranular cracking observed in the crack growth stage. Crack advance direction is from bottom to top.

3.2 CGR behaviors for NWC and HWC conditions in BWR environments

The CF tests were performed under cyclic loading in the simulated NWC condition with 200 ppb DO, and in the simulated HWC condition (10 ppb DO + 160 ppb DH). Figures 6(a) and 6(b) show plots of crack length (mm) vs. time (h) for specimens tested either at a higher loading frequency (4×10^{-3} Hz) or at a lower loading frequency (4×10^{-4} Hz) respectively, for a period during which conditions changed from NWC to HWC and back to NWC. In these two figures, it can be observed that whether the water chemistry was NWC or HWC, the time-based CGR at the higher frequency (4×10^{-3} Hz) was always

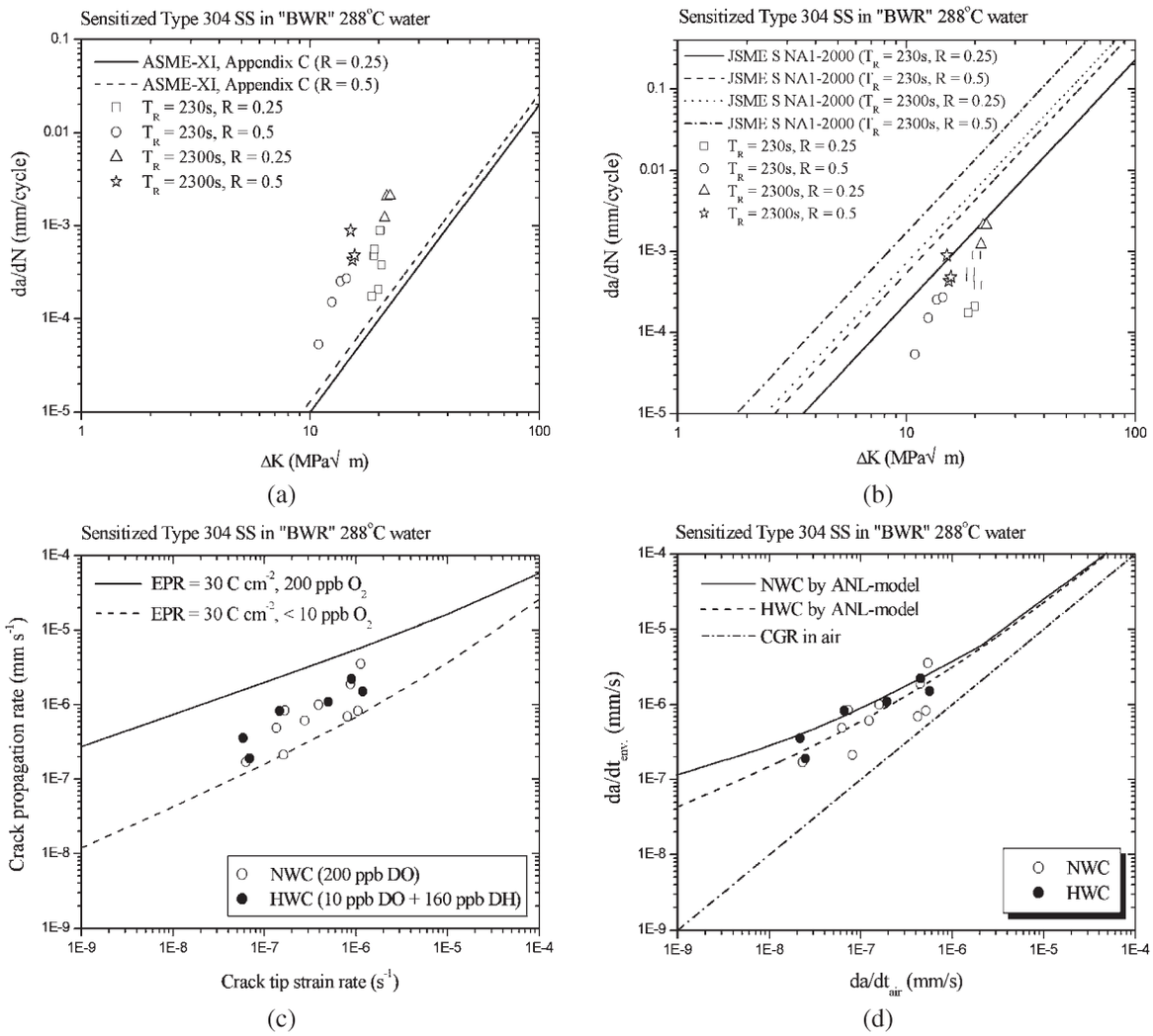

圖8　所有腐蝕疲勞裂縫成長速率之實驗數據與(a) ASME-XI, Appendix C[36]，(b) JSME S NA1-2000[37]，(c) GE-model[38~39]，以及(d) ANL-model[40~41]作比較。

Figure 8　All of the experimental corrosion fatigue CGR data compared to (a) ASME-XI, Appendix C[36], (b) JSME S NA1-2000[37], (c) GE-model[38~39], and (d) ANL-model[40~41].

more rapid than the CGR at the lower frequency (4×10^{-4} Hz) at a similar stress intensity factor range (ΔK) value and under the same water chemistry conditions. For example, at 4×10^{-3} Hz under NWC conditions, the CGR of one specimen (3.56×10^{-6} mm/s, ΔK = 20.29 MPa$\sqrt{m}$) was higher than that of a similar specimen (4.88×10^{-7} mm/s, ΔK = 21.22 MPa $\sqrt{m}$) tested at 4×10^{-4} Hz under NWC. In addition, in the HWC environment, the CGR (2.24×10^{-6} mm/s, ΔK = 19.13 MPa$\sqrt{m}$) tested at 4×10^{-3} Hz was also faster than that (8.31×10^{-7} mm/s, ΔK = 21.66 MPa $\sqrt{m}$) tested at 4×10^{-4} Hz. It is likely that the higher frequency resulted in a higher strain rate at the crack tip, which led to a higher CGR.

In addition, it is worth noting in Figures 6(a) and 6(b) that whether the loading frequency was high or low, the effect of the addition of 160 ppb H_2 on the CGR was not very large. In other words, adding a trace amount of H_2 could not suppress the CGR in this study. In contrast, in previous studies[56~57] we found that DH could effectively reduce the CGRs of reactor pressure vessel (RPV) LASs such as A508 Cl.2 (UNS K12766) and A533B (UNS K12539). In general, the effect of adding H_2 is to lower the ECP on the external surface of the steels. For SSs, it has been recognized that IGSCC is reduced markedly if the ECP can be decreased below a critical value of ~ -230 mV_{SHE}[58~60]. In the present study, even though the ECP was lowered to ~ -500 mV_{SHE} under HWC conditions (10 ppb DO + 160 ppb DH), as shown in Figure 6, the CGR was not reduced significantly.

The main reason that the ECP has little influence on CGR may be due to the solution conductivity. Andresen[61] reported that there is a large effect of solution conductivity such that raising the conductivity from ~ 0.1 to 0.4 μS/cm is equivalent to shifting from non-sensitized to sensitized SSs. Similarly, a reduction of water conductivity from 0.5 to 0.1 μS/cm can lower the CGR by a factor of ~ 13 times at 27.5 MPa$\sqrt{m}$, and this factor becomes even larger at lower stress intensities (crack tip strain rates)[61]. For sensitized SSs, the CGRs are generally much higher (up to two orders of magnitude) than those for non-sensitized SSs because the effect of chromium depletion on CGR can be quite marked and is much greater than the effects of grain-boundary segregation of phosphorus (P) or sulfur (S)[62]. However, in ultrahigh-purity water (e.g., outlet water conductivity < 0.1 μS/cm), Andresen and Briant [62] found that no effect of ECP on CGRs was observed over the range -500 to +250 mV_{SHE}. They also observed that additions of 150 ppb DH had no effect on CGRs in ultrahigh-purity (with very low conductivity) water[62]. Therefore, it is not difficult to speculate that the CGR in sensitized SSs will be similar to that in non-sensitized SSs if the former is tested in solutions of lower conductivity.

The assumption that DH cannot suppress the CGRs of sensitized SSs in high-purity water can be further confirmed by the results obtained from Ljungberg et al.[63]. They also found that there is no measurable effect on the CGRs in sensitized 304 SSs when switching from NWC to HWC under fatigue load conditions in high-purity water (0.08 to 0.12 μS/cm for NWC and 0.07 to 0.09 μS/cm for HWC). On the other hand, for some sensitized SSs tested in pure water with higher conductivity (≥ 0.3 μS/cm), the addition of H_2 to create HWC conditions was found to be beneficial in suppressing the CGRs[17, 64~66].

Whether the water chemistry was NWC or HWC, the fracture morphology was found to be mixed, as shown in Figure 7, with transgranular cracking (TGC) dominating in the precracking stage where a higher frequency was used. Predominantly intergranular cracking (IGC) was observed in the crack growth stage for a specimen immersed in high-temperature water.

3.3 CF-tests results in comparison with some predictive models

Figure 8(a) compares our CGR data to the reference curves of the ASME-XI, Appendix C[36], used to estimate the fatigue crack growth for austenitic SSs tested in air. It was found that none of the current data were encompassed by this code. The CGR data, which are higher than the ASME-XI, Appendix C reference curves, confirm the existence of the environmental effects in high-temperature water. In addition, it was observed that, at a longer rise time (2300 s), i.e., at a lower frequency, the CGRs exceed those in the reference curves by a factor of 6-12, whereas at a shorter rise time (230 s, or at a higher frequency), CGRs are only 2-6 times higher than those in the reference curves. Therefore, these results show that the reference curves of the ASME-XI, Appendix C are not conservative enough, and that the lower the loading frequency, the higher are the environmental effects on the CGR values.

The current ASME-XI reference CGR curves for austenitic SSs are only based on ΔK and R, and not on other variables that are known to be just as important, such as loading frequency (or rise time). Therefore, after sufficient experimental data were collected, new reference crack growth curves, the so-called JSME S NA1-2000 curves, were established by the JSME, which considered the significant effects of strain rate, loading frequency, and rise times. A comparison of the current CGR data with the JSME S NA1-2000 is shown in Figure 8(b). It is apparent that all of the current data are entirely encompassed by the JSME S NA1-2000 curves. However, it is worth noting that all of the experimental data are much lower than the predicted values by a factor of 4-13. Therefore, these results suggest that the JSME S NA1-2000 reference curves are overly conservative.

The GE-model[38] is primarily based on the slip-dissolution/film-rupture (SD/FR) mechanism. In this model, a crack advances as a result of the oxidation reactions occurring at the crack tip where a thermodynamically stable oxide (or protective film) is ruptured by an increase in the strain in the underlying matrix. The crack growth is mainly controlled by the crack-tip strain rate ($\dot{\varepsilon}_{ct}$), which governs the oxide film rupture frequency and the repassivation behavior after the film rupture event. In Figure 8(c), it can be observed that all of the current data tested under NWC (ECP ~ 50 mV_{SHE}) are lower than the reference curve of EPR = 30 C/cm^2 and 200 ppb O_2, whereas those tested under HWC (ECP ~ -550 mV_{SHE}) are higher than the reference curve of EPR = 30 C/cm^2 and < 10 ppb O_2. Consequently, this indicates that the GE-model fully encompasses the data for 304 SS tested under NWC conditions, but significantly underestimates the CGRs measured under HWC in simulated BWR environments.

In the GE-model, it is assumed that NWC and HWC conditions result in different ECP values on the surface of a stainless steel. Different ECPs will lead to different metal dissolution currents and therefore result in different CGRs. Hence, the CGR under NWC should be higher than that under HWC for a given crack-tip strain rate. However, in this study, it was observed that the CGRs under HWC were similar to, or even slightly higher than, those observed under NWC. This result suggests that the mechanism of cracking is not completely consistent with the SD/FR model for SSs tested under cyclic loading in simulated BWR environments. One possible reason that the GE-model underestimates CGRs under HWC is that different environments result in different oxide films, and the fracture strength of the oxide film formed under HWC is different from that formed under NWC. Therefore,

the CGRs are not only influenced by the dissolution current, which is dependent on the ECP, but also by the fracture strength of the protective oxide film.

Finally, we compare the current data with the ANL-model[40~41]. Basically, an estimation of the EAC rates in SSs by the ANL-model also relies on a superposition principle. The total CGR value ($(da/dt)_{total}$) includes the SCC rate ($\dot{a}_{scc}$) under constant load in the water environment, the CGR ($(da/dN)_{env}$) under cyclic load in the water environment, and the mechanical fatigue CGR ($(da/dN)_{air}$) tested in air. In addition, the difference between the ANL-NWC and the ANL-HWC equations is only based on the difference in the SCC CGR ($\dot{a}_{scc}$) values under constant loading. That is, the value of $\dot{a}_{scc}$can be assumed to be zero under HWC. The current CGR data are compared with the ANL-model[40~41] in Figure 8(d). This shows that, whether the specimens were tested under NWC or HWC, most of our CGR data are comparable with the values predicted by the ANL-model. Therefore, the present study indicates that the ANL-model is more suitable than the GE-model to predict the CGR values for sensitized SSs tested in simulated BWR environments.

3.4 Examination of the accuracy of the superposition principles developed by the GE-model and the ANL-model under cyclic or trapezoidal loading conditions

3.4.1 Evaluation of CGRs under cyclic loading

It is generally believed that the CF CGR under cyclic positive saw tooth loading is the superposition of the crack advance in air and the EAC during the rising load time period (Δt_R). However, the method used to assign a suitable weight to each parameter is still a controversial subject. In the GE-model, the CGRs in SSs are mainly controlled by the crack-tip strain rate ($\dot{\varepsilon}_{ct}$) based on a superposition principle as follows:

$$\frac{da}{dt} = A\dot{\varepsilon}_{ct}^{n} + 2\times10^{-2}\,\dot{\varepsilon}_{ct}^{1.0} \quad (4)$$

$$\dot{\varepsilon}_{ct} = 100 \times v \times A_R \times (\Delta K)^4 \text{ (for cyclic load)} \quad (5)$$

where da/dt is the CGR in cm/s, v is the loading frequency in Hz, A_R is a constant that is a function of the load ratio (R value), ΔK is the stress intensity factor range in ksi√in, and the values of A and n depend on the crack-tip material susceptibility (e.g., EPR values) and environmental factors such as conductivity and ECP values. The values of A and n ($A = 2\times10^{-4}$, n =0.429 for NWC and $A = 8\times10^{-5}$, n = 0.537 for HWC) were therefore selected according to the EPR value (30 C/cm^2) of the sensitized 304 SS used in this study.

On the other hand, the superposition model developed by ANL adopts the equations recorded in the report (NUREG-0313, Rev.2) published by the U.S. Nuclear Regulatory Commission (NRC)[67]. In this report, the CGRs in BWR environments containing 0.2 ppm or 8 ppm DO have been regulated. Because the SCC CGR () in PWR or in BWR/HWC environments is very low, it is ignored in the ANL-model. In addition, the EAC under cyclic loading is primarily based on the results obtained by Shoji et al.[68]. Shoji and coworkers considered that there exists a power law relationship between the time-based CGR in the water environment ($\dot{a}_{env}$) and that in air ($\dot{a}_{air}$), as follows:

$$\dot{a}_{env} = A(\dot{a}_{air})^m \quad (6)$$

where A and m are constants. Shoji et al. compared equation (6) with experimental data and determined that $A = 4\times10^{-5}$ and m = 0.5 in 288°C water containing 200 ppb DO, and that $A = 1.5\times10^{-4}$ and m = 0.5 in 288°C water containing 8 ppm DO. Therefore, the ANL-model[41] predicts the CGRs

under cyclic loading as follows:

$$\left(\frac{da}{dt}\right)_{total} = \frac{1}{\Delta t_R + \Delta t_F}\left[\,2\times\left(\frac{da}{dN}\right)_{air} + \left(\frac{da}{dt}\right)_{env}\times\Delta t_R + \left(\frac{da}{dt}\right)_{SCC}\times\Delta t_H\,\right]$$

$$= \frac{1}{\Delta t_R + \Delta t_F}\left[\,2\times\left(\frac{da}{dN}\right)_{air} + \left(\frac{da}{dN}\right)_{env} + \dot{a}_{SCC}\times\Delta t_H\,\right] \text{ (for NWC)} \qquad (7)$$

or

$$\left(\frac{da}{dt}\right)_{total} = \frac{1}{\Delta t_R + \Delta t_F}\left[\,2\times\left(\frac{da}{dN}\right)_{air} + \left(\frac{da}{dN}\right)_{env}\,\right] \text{ (for HWC or PWR)} \qquad (8)$$

where $(da/dt)_{total}$ is the total CGR in m/s, Δt_R is the rise time in seconds, Δt_H is the hold time in seconds, Δt_F is the fall time in seconds, $(da/dN)_{air}$ is the mechanical fatigue cycle-based CGR (m/cycle) tested in air, $(da/dN)_{env}$ is the cycle-based CGR (m/cycle) under a cyclic load in the water environment, and is the time-based CGR (m/s) under a constant (static) load in the water environment. The formulations of $\dot{a}_{scc}$, $(da/dN)_{air}$, and $(da/dN)_{env}$ are listed in Table 3.

3.4.2 Evaluation of CGRs under trapezoidal loading

The formulations of the CGR given in the previous section assumed cyclic loading without any hold time at maximum load. However, if the loading waveform changes from cyclic to trapezoidal (which includes a hold time), the GE-model predicts that the total crack advance is the sum of the crack advance attributed to mechanical fatigue, ($A_R(\Delta K)^4$), and EAC during the rising load time period (Δt_R) and EAC during the hold time (Δt_H) at maximum load[38]. This total crack advance can be converted to the average propagation rate by dividing it by the total cyclic time, i.e., $\Delta t_R + \Delta t_H + \Delta t_F$ (where Δt_F is the load fall time) as follows:

$$\left(\frac{da}{dt}\right)_{total} = \frac{1}{\Delta t_R + \Delta t_H + \Delta t_F}\left[\left(\frac{da}{dN}\right)_{air} + \left(\frac{da}{dt}\right)_{env}\times\Delta t_R + \left(\frac{da}{dt}\right)_{SCC}\times\Delta t_H\,\right]$$

$$= \frac{1}{\Delta t_R + \Delta t_H + \Delta t_F}\left[\,A_R(\Delta K)^4 + A(\dot{\varepsilon}_{rise-load})^n\times\Delta t_R + A(\dot{\varepsilon}_{static-load})^n\times\Delta t_H\,\right]$$

$$= \frac{1}{\Delta t_R + \Delta t_H + \Delta t_F}\left\{\,A_R(\Delta K)^4 + A\left[\frac{50}{\Delta t_R}(\Delta K)^4 A_R\right]^n\times\Delta t_R + A(6\times10^{-14}K^4_{\max})^n\times\Delta t_H\,\right]\right\} \qquad (9)$$

表3.　方程式(7)及(8)中$\dot{a}_{scc}$、$(da/dN)_{air}$與$(da/dN)_{env}$的公式。

Table 3　The formulations of $\dot{a}_{scc}$, $(da/dN)_{air}$, and $(da/dN)_{env}$ in equations (7) and (8).

Environment	NWC (200 ppb DO)	HWC
$\dot{a}_{SCC}$ (m/s)	$7.0\times10^{-14}\,K_{\max}^{2.161}$	0
$\left(\frac{da}{dN}\right)_{air}$ (m/c)	$3.43\times10^{-12}\times S(R)\times(\Delta K)^{3.3}$ $S(R) = 1.0 + 1.8R$ when $R \le 0.8$ $= -43.35 + 57.97R$ when $R > 0.8$	Same as NWC (200 ppb DO)
$\left(\frac{da}{dN}\right)_{env}$ (m/c)	$8.33\times10^{-11}\times S(R)^{0.5}\times\Delta t_R^{0.5}\times(\Delta K)^{1.65}$ $S(R) = 1.0 + 1.8R$ when $R \le 0.8$ $= -43.35 + 57.97R$ when $R > 0.8$	Same as NWC (200 ppb DO)

Note: K_{max} is the maximum stress intensity factor in MPa√m, R is the load ratio (K_{min}/K_{max}), and ΔK is the stress intensity factor range in MPa√m.

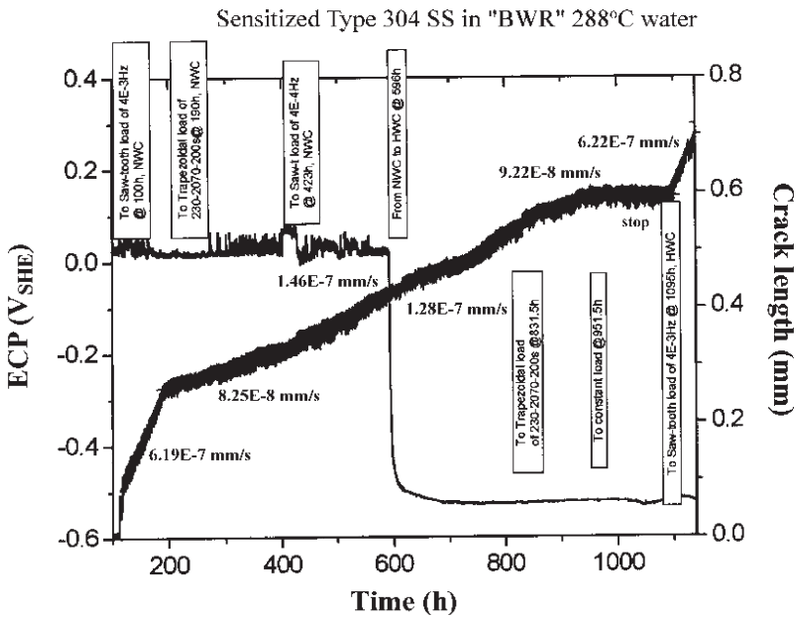

圖9　敏化之304型不銹鋼試片測試於往復式(頻率4×10^{-3}赫茲，4×10^{-4}赫茲)或梯形(上升時間230秒，維持時間2070秒)負荷的正常水化學/加氫水化學環境中，裂縫成長速率在288 °C水中隨時間的變化情形。

Figure 9　CGR as a function of time for a sensitized Type 304 SS specimen tested at 288 °C under cyclic (f = 4×10^{-3}, 4×10^{-4} Hz) or trapezoidal (Δt_R=230 s, Δt_H=2070 s) loadings in NWC/HWC environments.

where $(da/dt)_{total}$ is the total CGR in cm/s, Δt_R is the rise time in seconds, Δt_H is the hold time in seconds, Δt_F is the fall time in seconds, ΔK is the stress intensity factor range in ksi√in, K_{max} is the maximum stress intensity factor in ksi√in, and A_R is a constant that is a function of the load ratio (R value) as follows:

For $R < 0.42$, $A_R = 2.44\times10^{-11}$;
For $R \geq 0.42$, $A_R = -2.79\times0^{-11} + 1.115\times10^{-10}R + 5.5\times10^{-11}R^2$

Although the ANL-model provides predictive formulations (equations (7) and (8)) for cyclic loading, it is not clear how the ANL-model can be used to calculate the CGR under trapezoidal loading conditions. In this study, it is presumed that the weight of each parameter in the ANL-model is the same as that stipulated in the GE-model, but that the CGRs under different conditions ($(da/dN)_{air}$, $(da/dN)_{env}$, and $\dot{a}_{scc}$) are still determined by the formulations in the ANL-model, as listed in Table 3 Therefore, the CGRs under trapezoidal loading for the ANL-model can be evaluated as follows:

$$\left(\frac{da}{dt}\right)_{total} = \frac{1}{\Delta t_R + \Delta t_H + \Delta t_F}\left[\left(\frac{da}{dN}\right)_{air} + \left(\frac{da}{dt}\right)_{env}\times\Delta t_R + \left(\frac{da}{dt}\right)_{SCC}\times\Delta t_H\right]$$
$$= \frac{1}{\Delta t_R + \Delta t_H + \Delta t_F}\left[\left(\frac{da}{dN}\right)_{air} + \left(\frac{da}{dN}\right)_{env} + \dot{a}_{SCC}\times\Delta t_H\right] \quad (10)$$

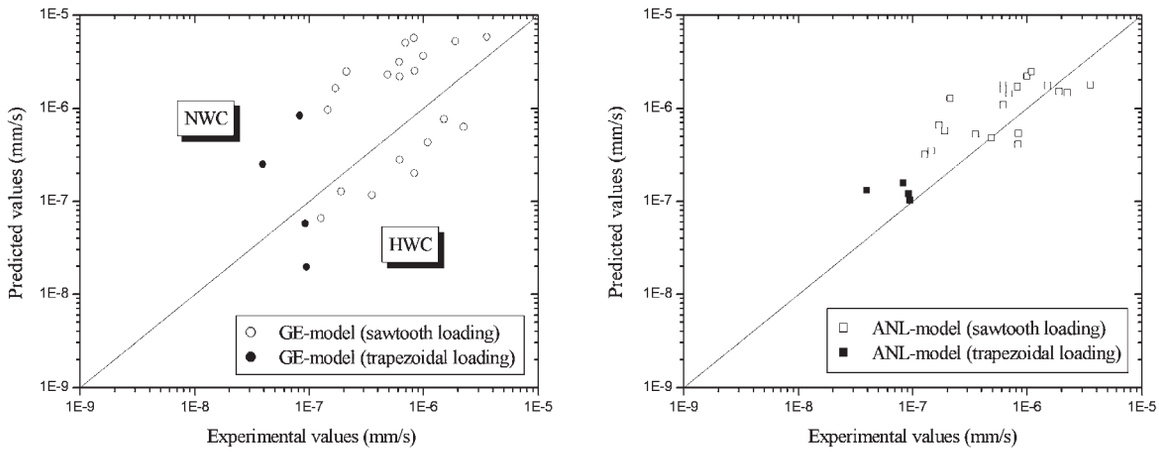

圖10　腐蝕疲勞裂縫成長速率之實驗數據與(a) GE模型以及(b) ANL模型所計算得的預測值相比較。結果顯示ANL模型的準確性較GE模型來得高。

Figure 10 Corrosion fatigue CGR experimental data compared with the predicted values calculated from (a) GE-model[38~39] and (b) ANL-model[40~41]. Results show that the accuracy of the ANL-model is higher than that developed by the GE-model.

3.5 Examination of the accuracy of the GE-model and the ANL-model

Figure 9 shows an example of combined CGR behaviors under either cyclic or trapezoidal loading in simulated BWR environments. Similar to the results for specimens tested under cyclic loading conditions, it was found that the addition of 160 ppb H_2 creating HWC could not suppress the CGR under trapezoidal loading (Figure 9). In this study, the CGRs measured under HWC conditions were not effectively reduced by DH and were even higher than those CGRs measured under NWC at a similar ΔK value and for the same loading waveform. For instance, with a rise-hold-fall waveform of 230 s 2070 s 200 s for one specimen tested under HWC conditions (Figure 9), the CGR of sensitized 304 SS (9.22×10^{-8} mm/s, ΔK = 12.12 MPa√m) was slightly higher than that (8.25×10^{-8} mm/s, ΔK = 11.49 MPa √m) tested under NWC. In addition, for another specimen tested under HWC with a waveform of 230 s-7200 s-200 s, the CGR (9.47×10^{-8} mm/s, ΔK = 12.17 MPa√m) was also higher than that (3.92×10^{-8} mm/s, ΔK = 10.71 MPa√m) tested under NWC conditions. By comparing the current CGR data under either cyclic or trapezoidal loading conditions with the values predicted by the GE-model (equations (4), (5), and (9)) and the ANL-model (equations (7), (8), and (10)), respectively as shown in Figures 10(a), and 10(b), we conclude that the accuracy of the predicted CGR values in the ANL-model is higher than that in the GE-model. In other words, whether the loading waveform is cyclic or trapezoidal, the current CGR data are close to the predicted values in the ANL-model. However, in the GE-model, all of the current CGR data are lower than the predicted values for specimens tested under NWC and slightly higher than the predicted values under HWC conditions. This indicates that the accuracy of the superposition principle (simple

addition) developed by the GE-model is lower than that assumed by the ANL-model.

4. Conclusions

Important features and conclusions drawn from the present study are summarized as follows:

1. There were no significant differences between the CGRs in sensitized 304 SS under HWC or NWC conditions in simulated BWR environments. It was found that HWC reduces CGRs very little under either cyclic or trapezoidal loading conditions.
2. Whether the loading waveform was positive saw tooth or trapezoidal, the accuracy of the ANL-model was higher than that of the GE-model. In the GE-model, the predicted CGR values for specimens tested under NWC were overestimated compared with the current data, whereas the predicted CGR values for specimens tested under HWC were slightly underestimated.
3. The current test CGR data cannot be encompassed by the disposition curve of the ASME Code Section XI, Appendix C. It was therefore shown that the ASME-XI, Appendix C is not conservative enough to predict the CGRs of austenitic SSs tested in high-temperature water, and that the lower the loading frequency, the larger the environmental effects are on the CGRs.
4. All of the current experimental CGR data are bounded by the JSME S NA1-2000 curves. However, the predicted values calculated from the JSME S NA1-2000 reference curves seem to be overly conservative.

References

1. T. Kondo, H. Nakajima, and R. Nagasaki, Nucl. Eng. Des., 16 (1971) 205.
2. T. Kondo, Y. Ogawa, and H. Nakajima, J. Electrochem. Soc., 21 (1974) 346.
3. "Stress Corrosion Cracking and Hydrogen Embrittlement of Iron-Base Alloys," presented in Firminy, France, June 1973, edited by R. W. Staehle, J. Hochmann, R. D. McCright, and J. E. Slatern, (Houston, TX: 1977).
4. Proc. 1st Int. Symp. on "Environmental Degradation of Materials in Nuclear Power Systems Water Reactors," held Aug. 1983 (Houston, TX: NACE, 1984).
5. Proc. 2nd Int. Symp. on "Environmental Degradation of Materials in Nuclear Power Systems Water Reactors," held Sept. 1985 (La Grange Park, IL: ANS, 1986).
6. Proc. 3rd Int. Symp. on "Environmental Degradation of Materials in Nuclear Power Systems Water Reactors," held Aug. 1987 (Washington, DC: AIME, 1988).
7. Proc. 4th Int. Symp. on "Environmental Degradation of Materials in Nuclear Power Systems Water Reactors," held Aug. 1989 (Houston, TX: NACE, 1990).
8. Proc. 5th Int. Symp. on "Environmental Degradation of Materials in Nuclear Power Systems Water Reactors," held Aug. 1991 (La Grange Park, IL: ANS, 1992).
9. Proc. 6th Int. Symp. on "Environmental Degradation of Materials in Nuclear Power Systems Water Reactors," held Aug. 1993 (Warrendale, PA: TMS, 1993).
10. Proc. 7th Int. Symp. on "Environmental Degradation of Materials in Nuclear Power Systems Water Reactors," held Aug. 1995 (Houston, TX: NACE, 1995).
11. Proc. 8th Int. Symp. on "Environmental Degradation of Materials in Nuclear Power Systems Water Reactors," held Aug. 1997 (La Grange Park, IL: ANS, 1997).
12. Proc. 9th Int. Symp. on "Environmental

Degradation of Materials in Nuclear Power Systems Water Reactors," held Aug. 1999 (Warrendale, PA: TMS, 1999).

13. Proc. 10th Int. Symp. on "Environmental Degradation of Materials in Nuclear Power Systems Water Reactors," held Aug. 2001 (Houston, TX: NACE, 2001).
14. Proc. 11th Int. Symp. on "Environmental Degradation of Materials in Nuclear Power Systems Water Reactors," held Aug. 2003 (La Grange Park, IL: ANS, 2003).
15. T. A. Prater, W. R. Catlin, and L. F. Coffin, "Effect of Hydrogen Additions to Water on the Corrosion Fatigue Behavior of Nuclear Structural Materials", Proc. 2nd Int. Symp. on "Environmental Degradation of Materials in Nuclear Power Systems Water Reactors," TMS, Breckenridge, Monterey, CA, September, 1985, p. 615.
16. R. L. Cowan, C. C. Lin, W. J. Marble, and C. P. Ruiz, "Hydrogen Water Chemistry in BWRs", Proc. 5th Int. Symp. on "Environmental Degradation of Materials in Nuclear Power Systems Water Reactors," (La Grange Park, IL: ANS, 1991), p. 50.
17. E. Kikuchi, M. Itow, J. Kuniya, H. Sakamoto, M. Yamamoto, A. Sudo, S. Suzuki, and M. Kitamura, Corrosion, 53 (1997) 306.
18. O. K. Chopra and D. J. Gavenda, "Effects of LWR Coolant Environments on Fatigue Lives of Austenitic Stainless Steels", ANL/ET/CP-91440, ASME Pressure Vessel and Piping Conference, Orlando, FL, USA , Jul. 27 Aug. 1, 1997 (Springfield, VA: NTIS, 1997).
19. O. K. Chopra and J. L. Smith, "Estimation of Fatigue Strain-Life Curves for Austenitic Stainless Steels in Light Water Reactor Environments", ANL/ET/CP-94714, Proceedings of the 1998 ASME/JSME Joint Pressure Vessel and Piping Conference, San Diego, CA, USA, Jul. 26-30, 1998 (Springfield, VA: NTIS, 1998).
20. M. Higuchi and K. Iida, "Reduction in Low-Cycle Fatigue Life of Austenitic Stainless Steels in High-Temperature Water", Pressure Vessel and Piping Codes and Standards, PVP Vol. 353, D. P. Jones, B. R. Newton, W. J. O' Donnell, R. Vecchio, G. A. Antaki, D. Bhavani, N, G. Cofie, and G. L. Hollinger, eds., ASME International, New York, 1997, p. 79.
21. W. A. Van Der Sluys and S. Yukawa, "Status of PVRC Evaluation of LWR Coolant Environmental Effects on the S-N Fatigue Properties of Pressure Boundary Materials", Fatigue and Crack Growth: Environmental Effects, Modeling Studies, and Design Considerations, PVP Vol. 306, S. Yukawa, ed., American Society of Mechanical Engineers, New York, p. 47.
22. W. A. Van Der Sluys and S. Yukawa, "S-N Fatigue Properties of Pressure Boundary Materials in LWR Coolant Environments", Proceedings of the 1998 ASME/JSME Joint Pressure Vessel and Piping Conference, San Diego, CA, USA, Jul. 26-30, 1998, PVP Vol. 374, S. Yukawa, ed., ASME, New York, p. 269.
23. O. K. Chopra and W. J. Shack, "Evaluation of Effects of LWR Coolant Environments on Fatigue Life of Carbon and Low-Alloy Steels", ANL/ET/CP-89613, ASTM Symposium on Effects of the Environment and the Initiation of Crack Growth, Orlando, FL, USA, May 20-21, 1996 (Springfield, VA: NTIS, 1996).
24. O. K. Chopra, "Environmental Effects on Fatigue Crack Initiation in Piping and Pressure Vessel Steels", ANL/ET/CP-101179, International Conference on Fatigue of Reactor Components, Napa, CA, USA, Jul. 31 Aug. 2, 2000 (Springfield, VA: NTIS, 2000).

25. R. P. Wei and J. D. Landes, Mater. Res. Standard, 9 (1969) 25.
26. I. M. Austen and E. F. Walker, “Quantitative Understanding of the Effects of Mechanical and Environmental Variables on Corrosion Fatigue Crack Growth Behaviour”, in: The Influence of Environment on Fatigue, Institution of Mechanical Engineers (I. Mech. E.) Conference Publications, London, 1977, p. 1.
27. S. P. Lynch, Met. Sci. J., 9 (1975) 401.
28. C. D. Beachem, Metall. Trans., 3 (1972) 437.
29. S. P. Lynch, in: “Fatigue Mechanisms”, ASTM-STP-675, edited by J. T. Fong (Philadelphia, PA: ASTM, 1979), p. 174.
30. S. P. Lynch, in: “Hydrogen Effects in Metals”, edited by A. W. Thompson and I. M. Bernstein, (New York, NY: AIME, 1981), p. 863.
31. T. Kawakubo, M. Hishida, K. Amano, and M. Katsuta, Corrosion, 36 (1980) 638.
32. N. J. H. Holroyd and D. Hardie, Corros. Sci., 23 (1983) 527.
33. W. Y. Maeng, Y. H. Kang, T. W. Nam, S. Ohashi, and T. Ishihara, J. Nucl. Mater., 275 (1999) 194.
34. D. V. Ramsamooj and T. A. Shugar, Int. J. Fatigue, 23 (2001) 301.
35. Y. Katada and S. Ohashi, “CF/SCC Interaction on Structural Materials for LWR in High Temperature Water”, Pressure Vessel and Piping Codes and Standards, PVP Vol. 439, ASME International, New York, 2002, p. 165.
36. ASME Boiler and Pressure Vessel Code, Section XI, Rules for Inservice Inspection of Nuclear Power Plant Components, Appendix C, “Evaluation of Flaws in Austenitic Piping”, the American Society of Mechanical Engineers, New York, 1995.
37. The Japan Society of Mechanical Engineers (JSME), “Rules on Fitness-for-Service for Nuclear Power Plants”, JSMESNAI-2000, p. 6-13, (2000).
38. F. P. Ford, D. F. Taylor, P. L. Andresen, and R. G. Ballinger, “Corrosion-Assisted Cracking of Stainless and Low-Alloy Steels in LWR Environments”, EPRI Contract RP2006-6, Final Report, NP-5064-M, Electric Power Research Institute, February 1987.
39. F. P. Ford and P. L. Andresen, ”Development and Use of a Predictive Model of Crack Propagation in 304/316L, A533B/A508 and Inconel 600/182 Alloys in 288 °C Water”, Third International Symposium on Environmental Degradation of Materials in Nuclear Power Systems – Water Reactors, Edited by G. J. Theus and J. R. Weeks, The Metallurgical Society (TMS), 1988, p. 789.
40. W. J. Shack and T. F. Kassner, “Review of Environmental Effects on Fatigue Crack Growth of Austenitic Stainless Steels”, NUREG/CR-6176, NRC, May 1994.
41. Workshop on Flaw Growth in Austenitic and Nickel-Based Materials, August 1, 2002, Snowbird, Utah, USA.
42. Japan Industrial Standard G 0580, “Method of Electrochemical Potentiokinetic Reactivation Ratio Measurement for Stainless Steels” (Japan, JIS, 2003).
43. ASTM Standard, E 399 – 90, “Standard Test Method for Plane-Strain Fracture Toughness of Metallic Materials”, in Annual Book of ASTM Standards, Vol. 03.01 (West Conshohocken, PA: ASTM International, 1998), p. 413.
44. L. W. Niedrach, J. Electrochem. Soc., 129 (1982) 145.
45. S. Ritter and H. P. Seifert, “Strain-Induced Corrosion Cracking of Low-Alloy Reactor Pressure Vessel Steels under BWR Conditions”, CORROSION/2002, paper no. 02516 (Houston, TX: NACE, 2002), p. 1.
46. P. L. Andresen, “Effects of testing characteristics

on observed SCC behavior in BWRs", CORROSION/98, paper no. 137 (Houston, TX: NACE, 1998), p. 137.1~137.16.

47. H. P. Seifert and S. Ritter, "Evaluation and Assessment of the BWR VIP 60 SCC Crack Growth Curves for Low-Alloy Steels under BWR/NWC Conditions", International Cooperative Group on Environmentally Assisted Cracking (ICG-EAC) Meeting, May 11-16, 2003, Ottawa, Canada.
48. ASTM Standard, E 647 – 95a, "Standard Test Method for Measurement of Fatigue Crack Growth Rates", in Annual Book of ASTM Standards, Vol. 03.01 (West Conshohocken, PA: ASTM International, 1998), p. 562.
49. J. Heldt and H. P. Seifert, Nucl. Eng. Des., 206 (2001) 57.
50. Y. J. Kim, "Role of Hydrogen Peroxide and Its Decomposition in BWRs", Tenth International Conference on Environmental Degradation of Materials in Nuclear Power Systems – Water Reactors, NACE/TMS/ANS, August 6-10, 2001, Lake Tahoe, Nevada, USA.
51. Y. J. Kim and P. L. Andresen, Corrosion, 59 (2003) 584.
52. D. D. Macdonald, H. Song, K. Makela, and K. Yoshida, Corrosion, 49 (1993) 8.
53. M. E. Indig and A. R. McIlree, Corrosion, 35 (1979) 288.
54. P. S. Maiya, T .F. Kassner, and W. E. Ruther, "Analysis of the Effects of Corrosion Potential and Impurities on the Stress Corrosion Cracking of Type 304 Stainless Steel", Second International Symposium on Environmental Degradation of Materials in Nuclear Power Systems – Water Reactors (Monterey, CA: ANS/TMS, 1985), p. 77.
55. C. C. Lin, F. R. Smith, N. Ichikawa, and M. Itow, Corrosion, 48 (1992) 16.
56. Y. Y. Chen, L. H. Wang, J. C. Oung, and H. C. Shih, Corrosion, 61 (2005) 273.
57. Y. Y. Chen, L. H. Wang, J. C. Oung, and H. C. Shih, unpublished data.
58. M. E. Indig, G. M. Gordon, and R. B. Davis, "The Role of Water Purity on Stress Corrosion Cracking", Proc. 1st Int. Symp. on "Environmental Degradation of Materials in Nuclear Power Systems Water Reactors," (Houston, TX: NACE, 1983), p. 506.
59. M. E. Indig, G. M. Gordon, R. B. Davis, and J. E. Weber, "Evaluation of In-Reactor Intergranular Stress Corrosion Cracking via Electrochemical Measurements", Proc. 2nd Int. Symp. on "Environmental Degradation of Materials in Nuclear Power Systems Water Reactors," (Houston, TX: NACE, 1985), p. 411.
60. L. G. Ljungberg, D. Cubicciotti, and M. Trolle, Corrosion, 42 (1986) 263.
61. P. L. Andresen, Corrosion, 44 (1988) 454.
62. P. L. Andresen and C. L. Briant, Corrosion, 45 (1989) 448.
63. L. G. Ljungberg, D. Cubicciotti, and M. Trolle, Corrosion, 46 (1990) 641.
64. E. Ibe, A. Watanabe, Y. Wada, and M. Takahashi, "Water Radiolysis near Metal Surfaces and Relevant Phenomena in Nuclear Reactor Systems", Proc. 6th Int. Conf. on "Water Chemistry of Nuclear Reactor Systems", Vol. 2 (London, U.K.: BNES, 1992), p. 73.
65. N. Ichikawa, Y. Hemmi, and J. Takagi, "Estimation on Corrosion Potential of Stainless Steels in BWR Primary Circuit", Proc. 6th Int. Conf. on "Water Chemistry of Nuclear Reactor Systems", Vol. 2 (London, U.K.: BNES, 1992), p. 127.
66. R. L. Jones, Mater. Perform., 30 (1991) 70.
67. W. S. Hazelton and W. H. Koo, "Technical Report on Material Selection and Process

Guidelines for BWR Coolant Pressure Boundary Piping", Final Report, NUREG-0313, Rev. 2, NRC, January 1988.

68. T. Shoji, S. Aiyama, H. Takahashi, and M. Suzuki, Corrosion, 34 (1978) 276.

收到日期：2005 年 8 月 25 日
修訂日期：2005 年 10 月 13 日
接受日期：2005 年 11 月 21 日